

## Coupling between charge movement and pore opening in vertebrate neuronal $\alpha_{1E}$ calcium channels

Riccardo Olcese\*, Alan Neely†, Ning Qin\*, Xiangyang Wei‡,  
Lutz Birnbaumer\*§ and Enrico Stefani\*¶¶

Departments of \*Anesthesiology, †Physiology and §Biological Chemistry,  
UCLA School of Medicine, Los Angeles, CA, ‡Department of Physiology, Texas Tech  
University Lubbock, TX and ¶Department of Molecular Medicine and Genetics,  
Medical College of Georgia, GA, USA

1. Neuronal  $\alpha_{1E}$   $\text{Ca}^{2+}$  channels were expressed alone and in combination with the  $\beta_{2a}$  subunit in *Xenopus laevis* oocytes.
2. The properties of ionic and gating currents of  $\alpha_{1E}$  were investigated: ionic currents were measured in 10 mM external  $\text{Ba}^{2+}$ ; gating currents were isolated in 2 mM external  $\text{Co}^{2+}$ .
3. Charge movement preceded channel opening. The charge movement voltage curve ( $Q(V)$ ) preceded the ionic conductance voltage dependence ( $G(V)$ ) by  $\sim 20$  mV.
4. Coexpression of  $\alpha_{1E}$  with the  $\beta_{2a}$  subunit did not modify the voltage dependence of charge movement but shifted the  $G(V)$  curve to more negative potentials. The voltage gap between  $Q(V)$  and  $G(V)$  curves was reduced by the  $\beta_{2a}$  subunit and both curves overlapped at potentials near 0 mV.
5. The coupling efficiency between the charge movement and pore opening was estimated by the ratio between limiting conductance and maximum charge movement ( $G_{\text{max}}/Q_{\text{max}}$ ). Coexpression of the  $\beta_{2a}$  subunit increased the  $G_{\text{max}}/Q_{\text{max}}$  ratio from  $9.2 \times 10^5 \pm 1.4 \times 10^5$  to  $21.9 \times 10^5 \pm 2.8 \times 10^5$  S  $\text{C}^{-1}$  for  $\alpha_{1E}$  and  $\alpha_{1E} + \beta_{2a}$ , respectively.
6. We conclude that in the neuronal  $\alpha_{1E}$  the charge movement is tightly coupled with the pore opening and that the  $\beta_{2a}$  subunit coexpression further improves this coupling.

Voltage-gated  $\text{Ca}^{2+}$  channels are composed of a pore forming  $\alpha_1$  subunit and one or more auxiliary subunits termed  $\beta$ ,  $\alpha_2\delta$  and  $\gamma$  (Catterall, 1991; Hofmann, Biel & Flockerzi, 1994). The  $\alpha_1$  subunit possesses the voltage-sensing machinery (Perez-Reyes *et al.* 1989) while the other subunits can increase  $\text{Ca}^{2+}$  current amplitude by increasing the expression level or by facilitating channel opening. For example, the coexpression of the skeletal muscle type-S  $\text{Ca}^{2+}$  channel ( $\alpha_{1S}$ ) in murine fibroblasts with the skeletal muscle  $\beta$  ( $\beta_{1a}$ ) subunit resulted in an increase in the number of high-affinity dihydropyridine binding sites, and in channels that activated faster than channels lacking  $\beta$  subunits (Lacerda *et al.* 1991). This  $\text{Ca}^{2+}$  current potentiation by the coexpression of  $\beta$  subunits seems to be a general phenomenon for  $\text{Ca}^{2+}$  channel  $\alpha_1$  subunits (Singer, Biel, Lotan, Flockerzi, Hofmann & Dascal, 1991; Varadi, Lory, Schultz, Varadi & Schwartz, 1991; Hullin *et al.* 1992; Williams *et al.* 1992; Lory, Varadi, Slish, Varadi & Schwartz, 1993; Olcese *et al.* 1994; De Ward & Campbell, 1995; Perez-Garcia, Kamp & Marban, 1995; Kamp, Perez-Garcia & Marban, 1996). The

potentiation of  $\text{Ca}^{2+}$  current by coexpression of the  $\beta$  subunit with the  $\alpha_1$  subunit may occur without an increase in the number of expressed channels in the *Xenopus* oocyte expression system. In fact, coexpression of the cardiac type C  $\alpha_1$  ( $\alpha_{1C}$ ) with the type 2  $\beta$  subunit ( $\beta_{2a}$ ) showed that the presence of the  $\beta$  subunit stimulates  $\text{Ca}^{2+}$  channel opening by improving the coupling of the voltage sensor to the opening of the pore, causing a leftward shift of the conductance–voltage ( $G(V)$ ) relationship without detectable changes in the size, voltage dependence and time course of charge movement (Neely, Wei, Olcese, Birnbaumer & Stefani, 1993). Moreover, direct biochemical determinations of the  $\text{Ca}^{2+}$  channel  $\alpha_{1C}$  protein showed that its expression level was increased by coexpression with the  $\alpha_2\delta$  subunit, while it was not affected by coexpression with the  $\beta_{2a}$  subunit which greatly potentiated ionic currents (Shistik, Ivanina, Puri, Hosey & Dascal, 1995). On the other hand, similar experiments in *Xenopus* oocytes with a chimeric cardiac  $\alpha_{1C}$ /skeletal muscle  $\alpha_{1S}$   $\text{Ca}^{2+}$  channel coexpressed with the  $\beta_{2a}$  subunit showed that the current potentiation

¶¶ To whom correspondence should be addressed.

was associated with an increase in the charge movement, suggesting that for this clone, the increase in current was due to a larger number of expressed channels (Delbono, Golapakrishnan, Neely, Olcese, Birnbaumer & Stefani, 1994). Similarly, in a mammalian expression system (embryonic kidney cell line), ionic currents and charge movement were enhanced by coexpression of the  $\text{Ca}^{2+}$  channel  $\alpha_{1C}$  with the  $\beta_{1a}$  and  $\beta_3$  subunits (Kamp *et al.* 1996; Josephson & Varadi, 1996).

Together these results suggest that the potentiation by coexpression of the  $\beta$  subunit may result from an increase of either channel opening or the number of inserted  $\text{Ca}^{2+}$  channels and that the relative contribution of these mechanisms will depend on the type of  $\text{Ca}^{2+}$  channel subunit and on the expression system. We have recently demonstrated that coexpression of  $\beta$  subunits with the neuronal  $\alpha_{1E}$  in *Xenopus* oocytes shifted the  $G(V)$  curve to more negative potentials and that the effect of  $\beta$  subunits on channel activation was independent of the type or subtype of  $\beta$  subunit tested (Schneider *et al.* 1994; Olcese *et al.* 1994). As for the  $\alpha_{1E}$ , coexpression of the  $\beta$  subunit with the cardiac  $\alpha_1$  subunit ( $\alpha_{1C}$ ) also resulted in a shift of the  $G(V)$  curve to more negative potentials. This shift occurred without significant changes in the  $Q(V)$  curve or in the time course of gating current (Neely *et al.* 1993). In the cardiac  $\alpha_{1C}$  subunit, the voltage separation between the  $Q(V)$  and  $G(V)$  curves is severalfold larger, indicating the existence of multiple transitions between closed states preceding channel opening that contribute to charge movement. The shift in the  $G(V)$  curve without changes in the  $Q(V)$  curve indicated that modulation of  $\alpha_{1C}$  by the  $\beta$  subunit facilitated channel opening, by altering relatively uncharged transitions with undetectable contribution to the total charge movement. In this paper, we examine the mechanism of  $\text{Ca}^{2+}$  channel potentiation by coexpression of the  $\beta$  ( $\beta_{2a}$ ) subunit with the neuronal  $\text{Ca}^{2+}$  channel  $\alpha_{1E}$  subunit by simultaneously measuring charge movement and ionic currents and comparing the findings with the results obtained in cardiac  $\text{Ca}^{2+}$  channels that show a large voltage separation between the  $Q(V)$  and  $G(V)$  curves.

## METHODS

### RNA synthesis

We used the rabbit cardiac  $\alpha_{1C}$  and the neuronal  $\alpha_{1E}$  pore-forming subunits, and the rabbit accessory  $\beta_{2a}$  subunit (Wei, Perez-Reyes, Lacerda, Schuster, Brown & Birnbaumer, 1991; Perez-Reyes *et al.* 1992; Schneider *et al.* 1994). For better expression of  $\alpha_{1C}$ , the amino terminus deletion mutant ( $\Delta N60$ ) of  $\alpha_{1C3}$ , which yields larger  $\text{Ca}^{2+}$  currents without changes in function (Wei, Neely, Olcese, Stefani & Birnbaumer, 1996), was used instead of the wild type  $\alpha_{1C}$ . The  $\beta_{2a}$  subunit was subcloned into pAGA2 vector, derived from pGEM-3 (Promega, Madison, WI, USA) containing an alfalfa mosaic virus translational initiation site and a 3' poly A tail to facilitate the expression in *Xenopus* oocytes (Sanford, Codina & Birnbaumer, 1991; Wei *et al.* 1991). Briefly, the full length cDNA encoding rat  $\beta_{2a}$  was amplified by polymerase chain reaction (PCR)

from the original clone in pBS using Pfu DNA polymerase (Stratagene, La Jolla, CA, USA) and primers B2.1 (containing an *Nco*I site) and B2.2 (containing an *Xba*I site). The PCR product was digested with *Nco*I and *Xba*I and subcloned into pAGA2 vector digested with the same restriction enzymes. The correctness of the constructs was confirmed by DNA sequencing using the dideoxy chain termination method.

To synthesize cRNA, all of the constructs were linearized with *Hind*III, followed by treatment with 2 mg ml<sup>-1</sup> proteinase K and 0.5% SDS at 37 °C for 30 min to remove traces of activity. After two phenol-chloroform extractions and ethanol precipitation, the templates were suspended in diethyl pyrocarbonate (DEPC)-treated water to a final concentration of 0.5 µg µl<sup>-1</sup>, and cRNAs were *in vitro* synthesized at 37 °C for 1–2 h in a volume of 25 µl containing 40 mM Tris-HCl (pH 7.2), 6 mM MgCl<sub>2</sub>, 10 mM dithiothreitol, 0.4 mM each of adenosine triphosphate, guanosine triphosphate, cytosine triphosphate and uridine triphosphate, 0.8 mM 7-methyl guanosine triphosphate and 10 U T7 RNA polymerase (Boehringer Mannheim, Indianapolis, IN, USA). The transcription products were then extracted with phenol-chloroform, precipitated twice with ethanol, and suspended in DEPC-treated water to a concentration of 0.4 µg µl<sup>-1</sup>; 50 nl of cRNA containing either 0.2 µg µl<sup>-1</sup> of  $\alpha_1$  subunit or a mixture of 0.2 µg ml<sup>-1</sup> of  $\alpha_1$  subunit and 0.2 µg ml<sup>-1</sup> of  $\beta_{2a}$  was injected per oocyte.

### Oocyte preparation

Frogs were anaesthetized by immersion in water containing 0.15–0.17% tricaine methanesulphonate for about 20 min or until full immobility, and the ovaries were removed under sterile conditions by surgical abdominal incision. The animals were then killed by decapitation. The animal protocols were performed with the approval of the Institutional Animal Care Committee of the University of California, Los Angeles.

Before injection, oocytes were defolliculated by collagenase treatment (Sigma Type I, 2 mg ml<sup>-1</sup> for 40 min at room temperature). Oocytes were maintained at 19.5 °C in Barth solution. Recordings were done 4–12 days after the RNA injection.

### Recording techniques

The cut-open oocyte voltage clamp technique was used to record ionic and gating currents from oocytes expressing  $\alpha_{1C}$  and  $\alpha_{1E}$   $\text{Ca}^{2+}$  channels, alone or in combination with the regulatory  $\beta_{2a}$  subunit (Stefani, Toro, Perozo & Bezanilla, 1994). The external solution (recording chamber and guard compartments) had the following composition: 10 mM Ba<sup>2+</sup>, 96 mM Na<sup>+</sup>, 10 mM Hepes, titrated to pH 7.0 with methanesulphonic acid (MES). The lower chamber in contact with the fraction of the oocyte permeabilized with 0.1% saponin contained 110 mM potassium glutamate, 10 mM Hepes titrated to pH 7.0 with NaOH. Because oocytes expressing  $\text{Ca}^{2+}$  channels showed large outward Cl<sup>-</sup> current even with Ba<sup>2+</sup> as the charge carrier, all of the oocytes were injected before recording with 100–150 nl of BAPTA-Na<sub>4</sub> (50 mM) titrated to pH 7.0 with MES, to prevent activation of  $\text{Ca}^{2+}$ - and Ba<sup>2+</sup>-activated Cl<sup>-</sup> channels (Barish, 1983; Neely, Olcese, Wei, Birnbaumer & Stefani, 1994). For gating current measurement, the ionic current was blocked by replacing 10 mM Ba<sup>2+</sup> with 2 mM Co<sup>2+</sup>, which left the charge movement unaltered and caused no changes of surface potential. To remove contaminating non-linear charge movement related to the endogenous Na<sup>+</sup>,K<sup>+</sup>-ATPase of the oocytes (Rakovsky, 1993), 0.1 mM ouabain was added to all of the external solutions. Leakage and linear capacity currents were compensated analogically and subtracted on-line using a *P/-4* subtraction

protocol from  $-120$  mV holding potential (SHP). Charge movement was detected for depolarization more positive than  $-70$  mV and was not changed by SHPs of  $-120$  or  $-90$  mV. These results indicate that negative subtracting pulses from  $-120$  mV SHP are adequate to subtract linear components.

Signals were filtered with an eight-pole Bessel filter to 1/5 of the sampling frequency. All of the experiments were performed at room temperature ( $22$ – $23$  °C).

## RESULTS

### Comparison of $\alpha_{1E}$ and $\alpha_{1C}$ ionic and associated gating currents

Figure 1 shows traces of  $\alpha_{1E}$  (upper panel) and  $\alpha_{1C}$  (lower panel) currents in  $10$  mM external  $\text{Ba}^{2+}$  for pulses to  $-30$ ,  $0$  and  $+30$  mV from a holding potential ( $V_h$ ) of  $-90$  mV. The recordings illustrate small transient upward deflections at the beginning of the voltage pulses that correspond to the gating currents (ON gating current). This initial ON gating current is followed by inward  $\text{Ba}^{2+}$  currents for pulses to  $0$  and  $+30$  mV. At the termination of the pulses, the  $\text{Ba}^{2+}$  current jumps to a large negative value due to the abrupt increase in the  $\text{Ba}^{2+}$  driving force. This so-called tail current decays as the channels close at the return potential. A salient difference between the  $\alpha_{1E}$  and  $\alpha_{1C}$  clones is that, for

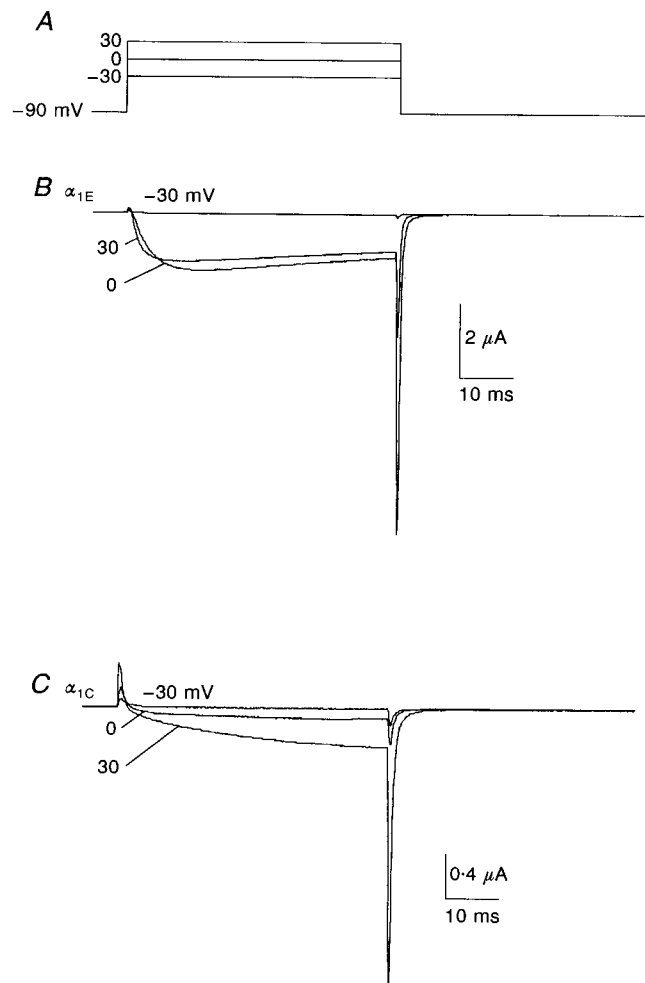
a similar current size of the inward current during a depolarizing step, the ON gating current is much smaller in the neuronal  $\alpha_{1E}$  channel than in the cardiac  $\alpha_{1C}$  subunit. The much smaller ratio between gating and ionic currents in  $\alpha_{1E}$  than in  $\alpha_{1C}$  suggests that pore opening in  $\alpha_{1E}$  is more efficiently coupled to the movement of the voltage sensor than in  $\alpha_{1C}$ . Thus for an equivalent amount of charge moved, a larger fraction of channels will open in  $\alpha_{1E}$  than in  $\alpha_{1C}$ .

### Isolation of ionic and gating currents

The records in Fig. 2 illustrate simultaneous recordings of ionic and gating currents of  $\alpha_{1E}$ . In Fig. 2A, B and C, superimposed current traces obtained from the same oocyte in  $10$  mM  $\text{Ba}^{2+}$  and  $2$  mM  $\text{Co}^{2+}$  are shown. Under both ionic conditions the voltage step to  $-30$  mV (Fig. 2A) elicited small transient outward and inward currents at the beginning and at the end of the pulse, respectively. These transient currents correspond to ON and OFF gating currents and remain unmodified by replacing  $10$  mM  $\text{Ba}^{2+}$  with  $2$  mM  $\text{Co}^{2+}$  in the external solution. Larger depolarizations to  $0$  and  $+30$  mV (Fig. 2B and C) elicited an initial ON gating current followed by the inward  $\text{Ba}^{2+}$  current. At the end of the pulse, the change in membrane potential induced a large inward tail current, mainly due to inward movement of  $\text{Ba}^{2+}$  which makes the much smaller

**Figure 1.** Ionic and gating current in  $\alpha_{1E}$  and  $\alpha_{1C}$  calcium channels

The records show the time course of ionic and gating current in  $\alpha_{1E}$  and  $\alpha_{1C}$   $\text{Ca}^{2+}$  channels.  $\text{Ba}^{2+}$  currents ( $10$  mM BaMES) are elicited by voltage steps to  $-30$ ,  $0$  and  $+30$  mV from a holding potential ( $V_h$ ) of  $-90$  mV. Note the dissimilar ratio between gating and ionic current in the two clones. All external solutions contain  $0.1$  mM ouabain in order to block the endogenous  $\text{Na}^+$ ,  $\text{K}^+$ -ATPase which produces non-linear charge movement under voltage steps.



gating current undetectable. To isolate gating currents, we replaced 10 mM  $Ba^{2+}$  in the external solution with 2 mM  $Co^{2+}$ . This ionic substitution blocked ionic current allowing the recording of gating current (Fig. 2*B* and *C*). As shown in Fig. 2*A*, *B* and *C*, the gating currents remained unmodified when 10 mM  $Ba^{2+}$  was replaced with 2 mM  $Co^{2+}$ , thus suggesting that this replacement does not alter the voltage dependence of charge movement. In Fig. 2*D*, *E* and *F* the charge conservation in ON and OFF gating currents is illustrated by evaluating their time integrals.

In the tail current, the relative contribution of ionic and gating current varies with the fraction of channels reaching the open state. At  $-30$  mV, primarily the OFF gating currents contributed to the tail current. With larger depolarizations, as more and more channels reach the open state, an increasing fraction of the tail current will reflect ionic current. To obtain the ionic component of the tail current, we subtracted the current traces measured in  $Co^{2+}$  from the ones obtained in  $Ba^{2+}$ . The same procedures to isolate ionic and gating currents were applied to the cardiac  $\alpha_{1C}$  and  $G(V)$  curves were constructed from the  $Co^{2+}$ -subtracted tail currents.

### Conductance–voltage ( $G(V)$ ) curves from tail current measurement

Figure 3 illustrates recordings to obtain  $G(V)$  curves from  $\alpha_{1E}$  channels. Depolarizing test pulses of 25 ms duration were delivered from  $-88$  to  $+132$  mV in 4 mV incremental steps from a  $V_h$  of  $-90$  mV. Currents were recorded in 10 mM  $Ba^{2+}$  (Fig. 3*B*) and after its replacement by 2 mM  $Co^{2+}$  (Fig. 3*C*). Figure 3*D* shows  $Co^{2+}$ -subtracted currents. The traces in Fig. 3*E* obtained in control oocytes at a similar gain show the virtual lack of endogenous currents in 10 mM external  $Ba^{2+}$  or 2 mM  $Co^{2+}$ . We consistently observed large outward current for depolarizations more positive than 70 mV in oocytes expressing  $Ca^{2+}$  channels. These outward currents were never detected in control oocytes in the same ionic conditions, indicating that they probably resulted from internal cations moving outwardly via the opened  $Ca^{2+}$  channels (Lee & Tsien, 1982).

While the inward  $Ba^{2+}$  currents were eliminated with 2 mM external  $Co^{2+}$ , the outward currents were partially blocked with external  $Co^{2+}$  (Fig. 3*C*, right panel) possibly by a release of the  $Co^{2+}$  block by the depolarization and the outward ion flux. This block is nearly instantaneously restored at the

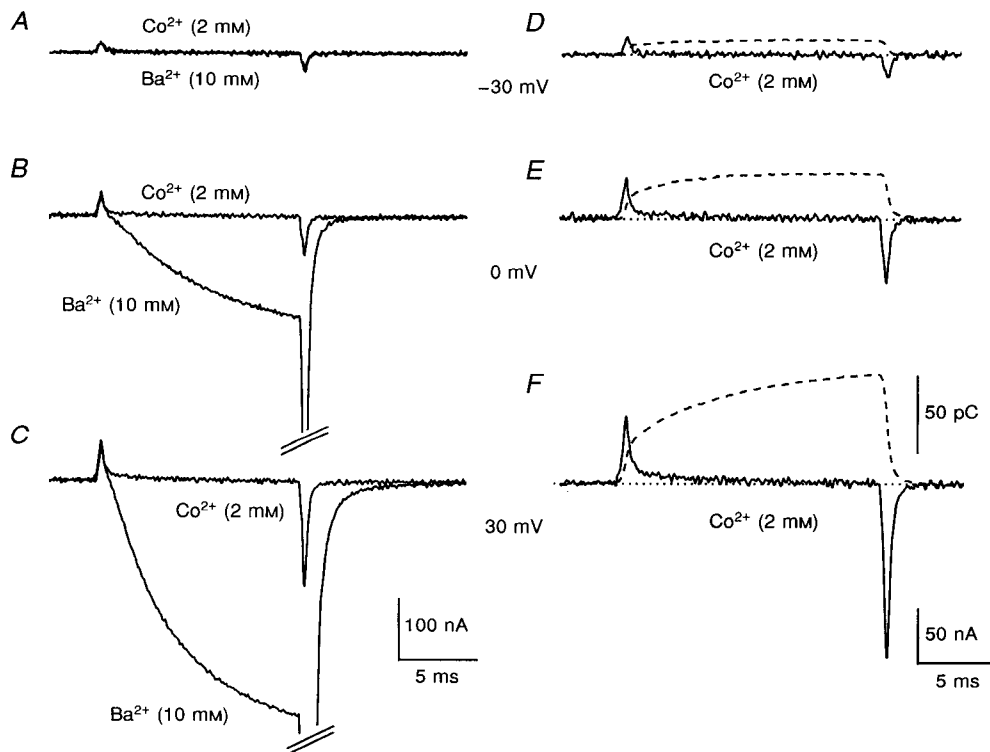


**Figure 2.** Gating current measurement

Separation of ionic and gating current on an  $\alpha_{1E}$  injected oocyte. *A*, *B* and *C* show membrane currents evoked by depolarizations to  $-30$ ,  $0$  and  $+30$  mV. For each potential, current traces recorded in 10 mM  $Ba^{2+}$  and 2 mM  $Co^{2+}$  are shown superimposed. The replacement of 10 mM  $Ba^{2+}$  by 2 mM  $Co^{2+}$  completely blocks the ionic current leaving the ON gating current unmodified. In *D*, *E* and *F*,  $\alpha_{1E}$  gating currents recorded at the indicated potentials, and their time integrals (dashed lines), are shown.

$-50$  mV return potential as shown by the absence of inward tail currents. Macroscopic conductance can be derived from macroscopic current during the test pulse by dividing it by the driving force. In our experiments, as revealed by the large outward current at very positive potentials, there is a significant asymmetry in the nature and relative selectivity of ions moving inward and outward through the expressed  $\text{Ca}^{2+}$  channels, and so this method was not applied. As pointed out by Bean & Rios (1989), an alternative approach that circumvents this problem is to measure peak tail currents at constant voltage following the various test potentials. The plot of peak tail current amplitude at a constant post-pulse potential as a function of a test potential yields the voltage dependence for the steady state

activation curve for the  $\text{Ca}^{2+}$  channel. We measured tail currents at  $-50$  mV since their decay is slow enough to allow for reliable measurements of their peak values. To ensure that only ionic current through  $\text{Ca}^{2+}$  channels were included, the peak tail current measurements were done over traces that were subtracted from traces recorded in  $2$  mM  $\text{Co}^{2+}$ . The measurement of the  $G(V)$  relationship from peak tail currents is accurate since it is obtained at a constant potential with a constant single channel amplitude and it is not contaminated with outward ionic current.

#### Effect of $\beta$ subunit coexpression on $\alpha_{1E}$ $G(V)$ curve

Figure 4 shows  $G(V)$  curves for  $\alpha_{1E}$  and  $\alpha_{1E} + \beta_{2a}$  fitted by the sum of two Boltzmann distributions (upper panel) and the averaged values of the parameters obtained fitting

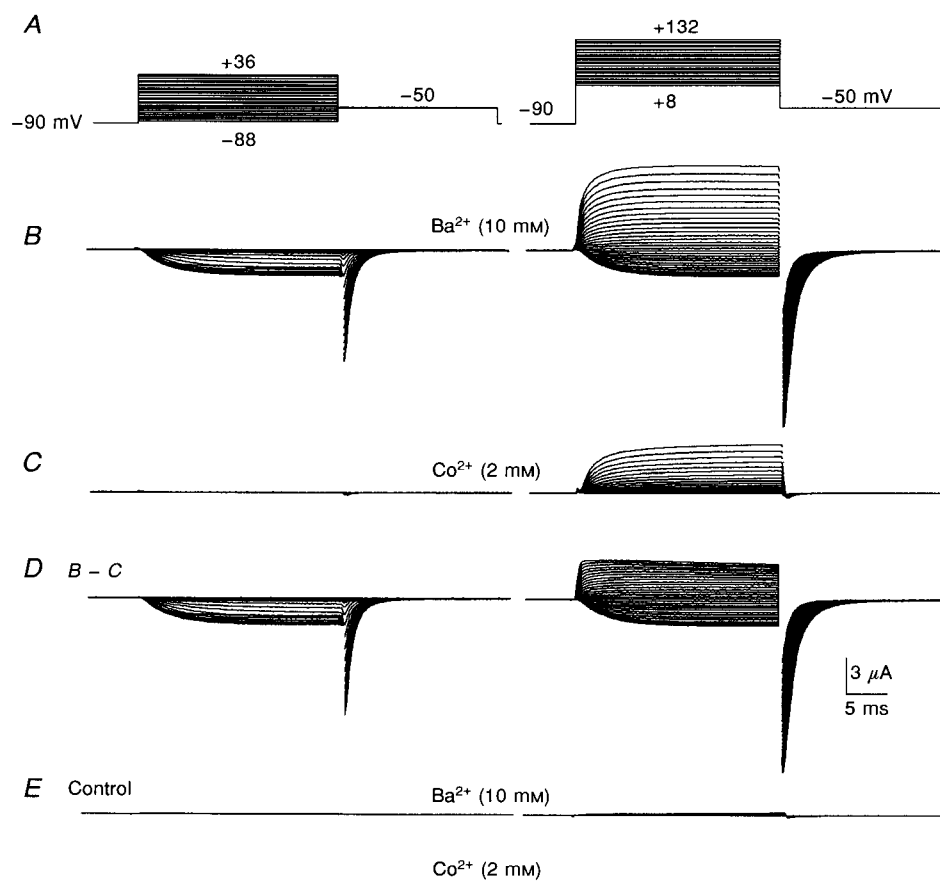


**Figure 3. Tail current measurement from  $\alpha_{1E}$  channels**

Non-linear membrane current measured in  $10$  mM  $\text{Ba}^{2+}$  (*B*) and in  $2$  mM  $\text{Co}^{2+}$  (*C*). The pulse protocol is displayed above the traces and is split into two parts covering a range of potentials from  $-88$  to  $+132$  mV in  $4$  mV increments (*A*). The slow decay of the tail current is due to the relatively high returning potential of  $-50$  mV. In  $2$  mM external  $\text{Co}^{2+}$  the inward current is totally removed (*C*) with the exception of the gating current. The outward current, still present at very positive potentials in the records with  $\text{Co}^{2+}$ , is due to the knock off of the  $\text{Co}^{2+}$  by the aspecific outward ion flux through the  $\text{Ca}^{2+}$  channels (*D*). As indicated by the absence of inward tail current, the block is promptly restored at the repolarization to  $-50$  mV. In *D*,  $\text{Co}^{2+}$ -subtracted  $\text{Ba}^{2+}$  currents used for the measurement of the  $G(V)$  relationship from the tail current are shown. In control oocytes (non-injected) at the same gain, no current is detected with  $10$  mM  $\text{Ba}^{2+}$  or  $2$  mM  $\text{Co}^{2+}$  in the external solution (*E*), meaning that all the outward current in the injected oocytes is carried by the expressed  $\text{Ca}^{2+}$  channels.

individual experiments (lower panel). Both  $G(V)$  curves can be empirically separated into two components described by the sum of two Boltzmann distributions. Averaged data points were fitted by:

$$\begin{aligned} G_m/G_{\max} = & (G_1/G_{\max})/\{1 + \exp[z_1(V_{1\text{half}} - V_m)(F/RT)]\} \\ & + (G_2/G_{\max})/\{1 + \exp[z_2(V_{2\text{half}} - V_m)(F/RT)]\}, \end{aligned}$$

where  $G_m$ ,  $G_1$  and  $G_2$  are the conductance values as a function of the prepulse potential  $V_m$ , and  $G_{\max}$  is the limiting conductance with the largest prepulse potential (+132 mV). The conductance was measured from tail currents at  $-50$  mV by dividing the peak tail current by the effective  $\text{Ba}^{2+}$  driving force ( $-50 - E_{\text{Ba}} = -110$  mV).  $V_{1\text{half}}$  and  $V_{2\text{half}}$  are the half-activation potentials,  $z_1$  and  $z_2$  are the effective valences, and  $F$ ,  $R$  and  $T$  (295 K) are the usual thermodynamic parameters. Similar values were obtained for the equivalent effective valences and half-activation

potentials for each component of the Boltzmann distribution fitting  $\alpha_{1E}$  and  $\alpha_{1E} + \beta_{2a}$ . The difference in the Boltzmann distributions that fitted the  $\alpha_{1E}$  and  $\alpha_{1E} + \beta_{2a}$   $G(V)$  data was found to reside in the relative proportion of their amplitude factors  $G_1/G_{\max}$  and  $G_2/G_{\max}$ . For  $\alpha_{1E}$   $G(V)$  curves, both components had a similar weight, while for  $\alpha_{1E} + \beta_{2a}$   $G(V)$  curves, the component with the more negative half-activation potential and steeper voltage dependence became predominant, explaining the overall negative shift in the  $G(V)$  curve.

#### Charge movement and $\text{Ba}^{2+}$ currents of $\alpha_{1E}$ and $\alpha_{1E} + \beta_{2a}$ $\text{Ca}^{2+}$ channels

Figure 5 illustrates ionic (upper panel) and gating currents (lower panel) of  $\alpha_{1E}$  (left panel) and  $\alpha_{1E} + \beta_{2a}$  (right panel)  $\text{Ca}^{2+}$  channels. Coexpression of the  $\beta_{2a}$  subunit has no major effect on the activation time constant ( $\tau$ ). The time constant ( $\tau$ ) of the  $\text{Ba}^{2+}$  current activation for depolarizations to

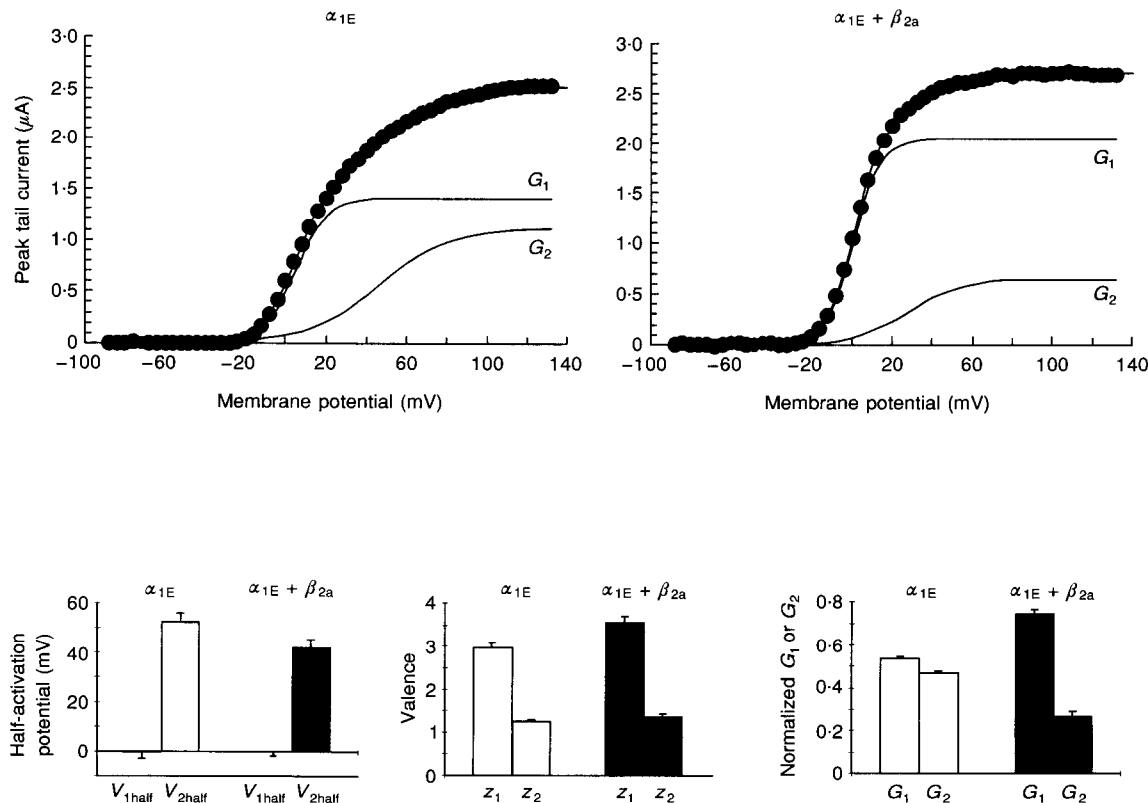


**Figure 4.**  $\beta$  Subunit facilitates channel opening changing the ratio of the two component of the  $G(V)$  curve

The upper panel shows representative  $\alpha_{1E}$  and  $\alpha_{1E} + \beta_{2a}$  conductance–voltage curves ( $G(V)$ ) from peak tail currents (external  $\text{Ba}^{2+}$  10 mM) during repolarization to  $-50$  mV. Data points are fitted by the sum of two Boltzmann distributions (continuous line) and the two components  $G_1$  and  $G_2$  are displayed separately. The lower panel shows bar plots of the averaged parameters fitting the individual  $G(V)$  curves: for  $\alpha_{1E}$ :  $G_1 = 0.53 \pm 0.01$  mV,  $z_1 = 2.9 \pm 0.1$ ,  $V_{1\text{half}} = -0.3 \pm 2.1$  mV,  $G_2 = 0.47 \pm 0.01$ ,  $z_2 = 1.3 \pm 0.04$ ,  $V_{2\text{half}} = 52.4 \pm 3.6$  mV; and for  $\alpha_{1E} + \beta_{2a}$ :  $G_1 = 0.74 \pm 0.02$ ,  $z_1 = 3.6 \pm 0.1$ ,  $V_{1\text{half}} = -0.2 \pm 1.0$  mV,  $G_2 = 0.26 \pm 0.01$ ,  $z_2 = 1.4 \pm 0.1$ ,  $V_{2\text{half}} = 41 \pm 3.0$  mV ( $n = 15$  for  $\alpha_{1E}$  and  $\alpha_{1E} + \beta_{2a}$ ). The coexpression of the  $\beta$  subunit seems to have little action on the half-activation potential ( $V_{1\text{half}}$  and  $V_{2\text{half}}$ ) and the effective valences ( $z_1$  and  $z_2$ ) of the components, while enhancing the first, more negative and steeper component of the  $G(V)$  ( $G_1$ ). Error bars are the standard errors of the mean.

16 mV was 3.1 and 2.7 ms for  $\alpha_{1E}$  and  $\alpha_{1E} + \beta_{2a}$ , respectively. The trace to +60 mV is at the ionic current reversal potential and shows the ON gating current. Note the proportionally smaller charge movement in relation to the  $\text{Ba}^{2+}$  current for the  $\alpha_{1E} + \beta_{2a}$  channel. Figure 5C and D show records of  $\alpha_{1E}$  and  $\alpha_{1E} + \beta_{2a}$  gating current elicited by voltage steps from a  $V_h$  of -90 mV to various potentials and demonstrates that the time courses of the  $\alpha_{1E}$  gating currents were not modified by  $\beta_{2a}$  coexpression.

In all batches of oocytes, coexpression of the  $\beta_{2a}$  subunit consistently induced a leftward shift of the  $G(V)$  curves, as shown in Fig. 4. This action was independent of the expression level which was variable. For example, in batches of oocytes with low expression of  $\alpha_{1E}$  ( $G_{\max} = 64 \pm 14 \mu\text{S}$ ,  $n = 5$ ), the  $\beta_{2a}$  subunit approximately doubled ionic currents ( $G_{\max} = 154 \pm 31 \mu\text{S}$ ,  $n = 5$ ), while in other batches of oocytes with high expression of  $\alpha_{1E}$ ,  $G_{\max}$  had similar values for  $\alpha_{1E}$  of  $123 \pm 14 \mu\text{S}$  ( $n = 20$ , from 10 batches) and for  $\alpha_{1E} + \beta_{2a}$  of  $82 \pm 19 \mu\text{S}$  ( $n = 14$ , from 7 batches of oocytes)

(Fig. 6A). In the same group of oocytes with high  $\alpha_{1E}$  expression, coexpression of  $\beta_{2a}$  reduced  $Q_{\max}$  (Fig. 6B). A better way to evaluate the action of the  $\beta_{2a}$  subunit on channel gating is to measure in the same oocyte the coupling efficiency between charge movement and pore opening by the  $G_{\max}/Q_{\max}$  ratio where  $Q_{\max}$  is the total charge moved.  $Q_{\max}$  was measured at the ionic reversal potential in 10 mM  $\text{Ba}^{2+}$  (Fig. 5A and B) and after blocking the  $\text{Ba}^{2+}$  currents with 2 mM  $\text{Co}^{2+}$ . The  $G_{\max}/Q_{\max}$  ratio was significantly higher for  $\alpha_{1E} + \beta_{2a}$  channels:  $\alpha_{1E} = 9.22 \times 10^5 \pm 1.4 \times 10^5 \text{ S C}^{-1}$  ( $n = 20$ ) and  $\alpha_{1E} + \beta_{2a} = 21.95 \times 10^5 \pm 2.8 \times 10^5$  ( $n = 14$ ) (Fig. 6C). Assuming that the  $\beta_{2a}$  subunit does not change the number of effective charges per channel, the higher coupling efficiency indicates that an equivalent number of channels measured by the  $Q_{\max}$  elicits larger currents when coexpressed with the  $\beta_{2a}$  subunit. Since the single channel amplitude was not affected by the  $\beta_{2a}$  subunit (Noceti *et al.* 1996), the ionic current potentiation should arise from an increase in channel openings. The fact that the potentiated  $\alpha_{1E} + \beta_{2a}$  currents have a time course that is very similar to

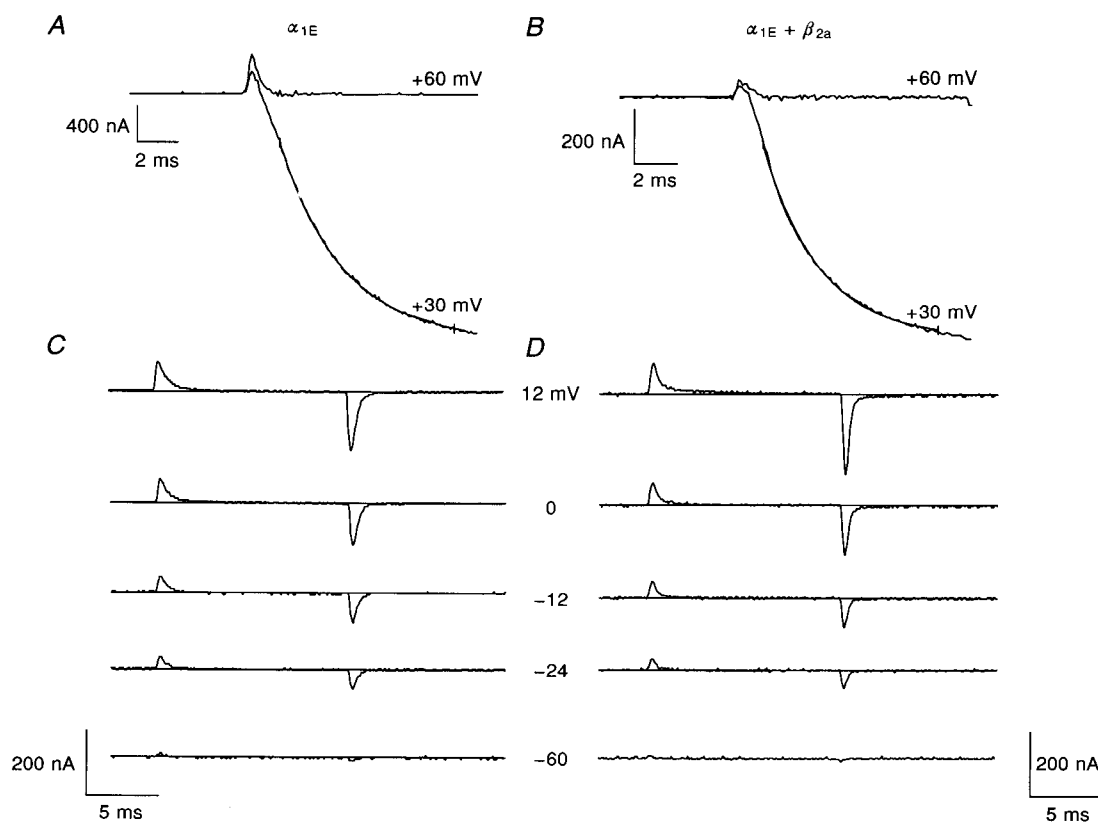


**Figure 5.** Gating current in  $\alpha_{1E}$

Upper panel shows current traces in 10 mM external  $\text{Ba}^{2+}$  elicited by depolarization to 30 and 60 mV in oocytes expressing  $\alpha_{1E}$  (A) and  $\alpha_{1E} + \beta_{2a}$  (B). The activation time constants, obtained by fitting the very early phases of the ionic current during depolarization to 30 mV to a single exponential function, are practically the same in the two clones (3.1 ms for  $\alpha_{1E}$  and 2.7 ms for  $\alpha_{1E} + \beta_{2a}$ ). Note the relative smaller size of charge movement which precedes the ionic current in the  $\alpha_{1E} + \beta_{2a}$  compared with  $\alpha_{1E}$  expressed alone. The lower panel shows  $\alpha_{1E}$  (C) and  $\alpha_{1E} + \beta_{2a}$  (D) gating currents (2 mM external  $\text{Co}^{2+}$ ) evoked by the indicated voltage steps from a holding potential ( $V_h$ ) of -90 mV. Subtracting protocol was  $P/-4$  from a  $V_h$  of -120.

that of the  $\alpha_{1E}$  currents strongly suggests that the main action of the  $\beta_{2a}$  subunit is to reduce the proportion of null traces.

#### Voltage dependence of charge movement and channel activation of $\alpha_{1E}$ and $\alpha_{1E} + \beta_{2a}$ $\text{Ca}^{2+}$ channels

To further evaluate the action of the  $\beta_{2a}$  subunit on pore opening of  $\alpha_{1E}$ , we plotted  $\log Q$  and  $\log G$  vs. the membrane potential (Fig. 7A). For comparison, equivalent plots for  $\alpha_{1C}$  and  $\alpha_{1C} + \beta_{2a}$  cardiac  $\text{Ca}^{2+}$  channels are illustrated in Fig. 7B. The plots show that coexpression of the  $\beta_{2a}$  subunit induces an overall shift of the  $G(V)$  curves to more negative potentials, with the characteristics described in Fig. 4, and that these changes in the  $G(V)$  curves were not associated with modifications in the  $Q(V)$  curve. The  $Q(V)$  relationships, obtained by plotting the time integral of the ON gating current vs. the membrane potential, were empirically fitted by sums of two Boltzmann distributions:

$$Q_{\text{on}}/Q_{\text{max}} = (Q_1/Q_{\text{max}})/\{1 + \exp[z_{q1}(V_{q1\text{half}} - V_m)(F/RT)]\} \\ + (Q_2/Q_{\text{max}})/\{1 + \exp[z_{q2}(V_{q2\text{half}} - V_m)(F/RT)]\},$$

where  $Q_{\text{max}}$  is the limiting charge movement,  $Q_1$  and  $Q_2$  are the amplitudes of the charge components,  $z_{q1}$  and  $z_{q2}$  are the effective valences and  $V_{q1\text{half}}$  and  $V_{q2\text{half}}$  are the respective half-activation potentials. The charge movement of  $\alpha_{1E}$  could be separated into two components with about the

same amplitude: the first had a shallower voltage dependence,  $z_{q1} = 1.42$  with  $V_{q1\text{half}} = -18$  mV; the second component had a steeper voltage dependence,  $z_{q2} = 3.3$  with  $V_{q2\text{half}} = 16$  mV. The  $Q(V)$  curve for  $\alpha_{1C}$  showed only one component with a voltage dependence practically identical to that of the first component of  $\alpha_{1E}$ . The coexpression of  $\beta$  subunits did not modify the voltage dependence of the charge movement of  $\alpha_{1E}$  or  $\alpha_{1C}$ . For  $\alpha_{1C}$  and  $\alpha_{1C} + \beta_{2a}$ , both  $Q(V)$  curves were virtually indistinguishable and were fitted by a single Boltzmann function with  $z = 1.52$  and  $V_{q\text{half}} = -17$  mV (for  $\alpha_{1C}$ ), and  $z = 1.44$  and  $V_{q\text{half}} = -20$  mV (for  $\alpha_{1C} + \beta_{2a}$ ). The  $G(V)$  curves for  $\alpha_{1C}$  and  $\alpha_{1C} + \beta_{2a}$  were fitted by the sum of two Boltzmann distributions with the following parameters.  $\alpha_{1C}$ :  $G_1/G_{\text{max}} = 0.54$ ,  $z_1 = 1.89$ ,  $V_{1\text{half}} = 69$  mV,  $G_2/G_{\text{max}} = 0.46$ ,  $z_2 = 1.52$ ,  $V_{2\text{half}} = 100$  mV; and  $\alpha_{1C} + \beta_{2a}$ :  $G_1/G_{\text{max}} = 0.30$ ,  $z_1 = 2.77$ ,  $V_{1\text{half}} = -3.9$  mV,  $G_2/G_{\text{max}} = 0.7$ ,  $z_2 = 1.38$ ,  $V_{2\text{half}} = 58$  mV.

For both the  $\alpha_{1E}$  and the  $\alpha_{1C}$  channels, the  $Q(V)$  curves are more negative in voltage axis than the  $G(V)$  curves indicating the existence of several closed states prior to channel opening. The voltage separation between  $Q(V)$  and  $G(V)$  curves is much larger in the  $\alpha_{1C}$  channels and the  $Q(V)$  curves of both channels were not affected by the coexpression of the  $\beta_{2a}$  subunit, which shifted the  $G(V)$  curves to more negative potentials.

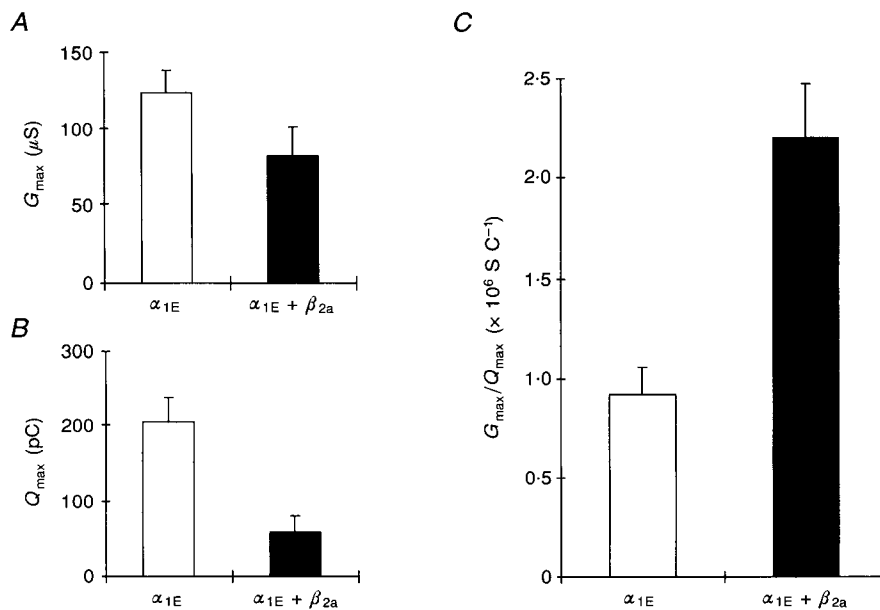


**Figure 6.** Coexpression of  $\beta_{2a}$  subunit improves the coupling efficiency in  $\alpha_{1E}$  channels

A, averaged membrane limiting conductance in 10 mM  $\text{Ba}^{2+}$  ( $G_{\text{max}}$ ) of oocytes expressing  $\alpha_{1E}$  and  $\alpha_{1E} + \beta_{2a}$ . The values are obtained by dividing the peak tail current at  $-50$  mV following a voltage step to  $+132$  mV by the  $\text{Ba}^{2+}$  driving force ( $E_m - E_{\text{Ba}} = -50 - (+60) = -110$  mV, where  $E_m$  is the membrane potential and  $E_{\text{Ba}}$  the apparent reversal potential for  $\text{Ba}^{2+}$ ). B, the limiting charge movement ( $Q_{\text{max}}$ ) for  $\alpha_{1E}$  and  $\alpha_{1E} + \beta_{2a}$  obtained by integrating the gating current at the reversal potential ( $\sim 60$  mV). The ratio  $G_{\text{max}}/Q_{\text{max}}$  for  $\alpha_{1E}$  and  $\alpha_{1E} + \beta_{2a}$  is shown in C. The coexpression of the  $\beta_{2a}$  subunit improved the coupling efficiency of  $\alpha_{1E}$  channels.

## DISCUSSION

Voltage gated ion channels are membrane proteins that react to changes in the electric field across the membrane by modifying their secondary and tertiary structures. Mild depolarizations lead the channel protein through sequential conformational changes that represent the structural rearrangement that prepares the whole protein for the last closed-to-open transition. Stronger depolarizations finally bring the channel to the conducting conformation. The transduction of the changes of membrane potential into structural modification of the channel protein is triggered by the voltage sensor which, behaving like an electrical dipole, reorients within the electric field and 'drags' the rest of the protein through the different conformational states.

The heavily charged fourth transmembrane segment of the voltage gated channels was the first candidate identified for the role of voltage sensor and its actual movement under the voltage field has been recently shown for the *Shaker*  $\text{K}^+$  channel (Mannuzzu, Moronne & Isacoff, 1996). The efficiency of the movement of the voltage sensor on driving the rest of the molecule toward the open conformation will be reflected in the biophysical properties of the channels such as the position of the  $G(V)$  curve relative to the  $Q(V)$  curve along the voltage axis. By comparing the properties of the neuronal  $\alpha_{1E}$  with the cardiac  $\alpha_{1C}$ , we have shown that in the neuronal channel a proportionally much smaller charge movement is required to elicit ionic current than in the cardiac channel (Fig. 1). One may think that this difference

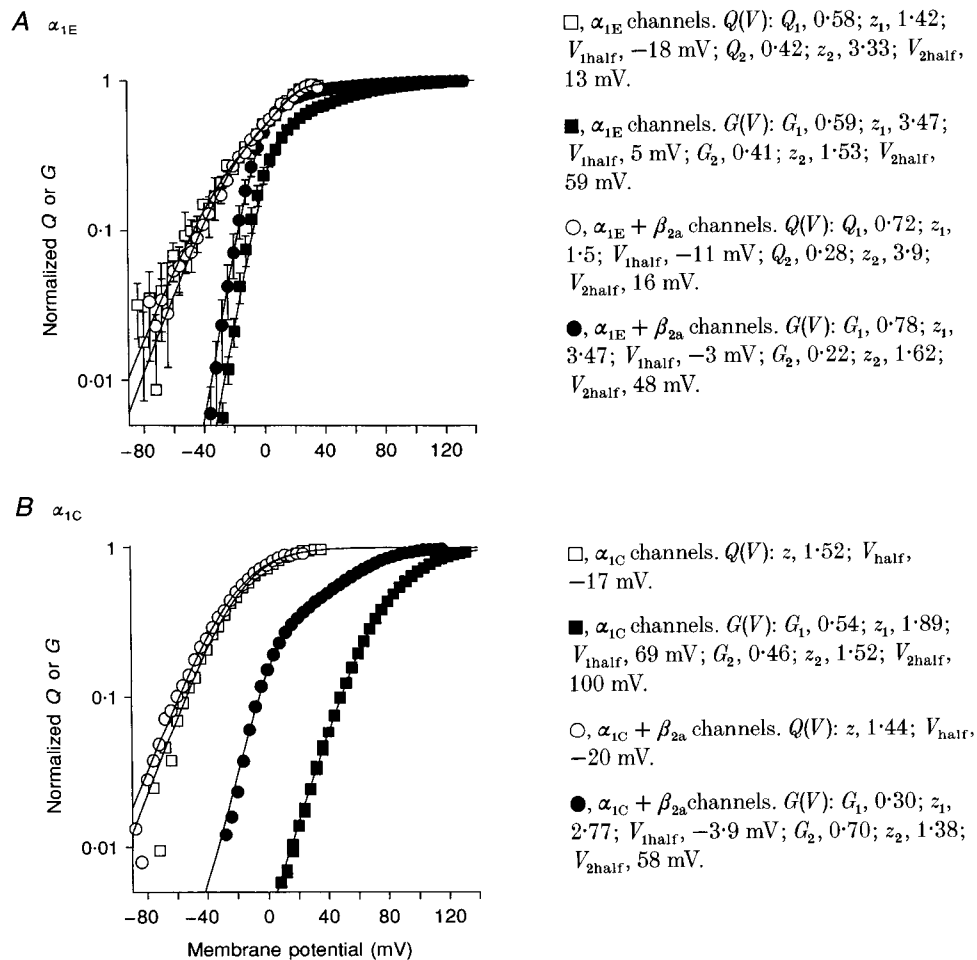


**Figure 7.** Coupling between charge movement and pore opening in  $\alpha_{1E}$  and  $\alpha_{1C}$   $\text{Ca}^{2+}$  channels

The figure shows (upper panel) the averaged voltage dependence of the charge movement for  $\alpha_{1E}$  (□), and  $\alpha_{1E} + \beta_{2a}$  channels (○), and the  $\text{Ba}^{2+}$  conductance for  $\alpha_{1E}$  (■) and  $\alpha_{1E} + \beta_{2a}$  channels (●); for comparison, an analogous semilogarithmic plot is shown for the cardiac  $\alpha_{1C}$  and  $\alpha_{1C} + \beta_{2a}$  channels (lower panel). Error bars are the standard errors of the mean ( $n = 3$ ). The  $G(V)$  and  $Q(V)$  curves for  $\alpha_{1C}$  channels are fitted to the sum of two Boltzmann distributions. Parameters fitting the experimental data are shown on the right-hand side:  $z_1$  and  $z_2$  are the effective valence,  $V_{1/2}$  and  $V_{2/2}$  are half-activation potentials,  $G_1$  and  $G_2$ ,  $Q_1$  and  $Q_2$  are the relative amplitude of the  $G(V)$  or  $Q(V)$  curves. The main difference between  $\alpha_{1E}$  and  $\alpha_{1C}$  channels is the voltage separation of their  $Q(V)$  and  $G(V)$  curves.

could be due to a different number of charges per channel in the two clones which have similar limiting maximal open probability. However, we have independent measurements indicating that  $\alpha_{1E}$  and  $\alpha_{1C}$  have a similar number of charges per channel (Noceti *et al.* 1996): about nine unitary charges per channel are estimated for both  $\alpha_{1E}$  and  $\alpha_{1C}$  using the limiting slope (Almers, 1978; Almers & Armstrong, 1980) and variance analysis (Schoppa, McCormack, Tanouye & Sigworth, 1992). Because of the equality of the number of charges per channel in the two clones, the difference in the channel efficiency must lie in the way the two voltage sensors are coupled to the channel opening; this is mainly reflected in the relative position of the  $G(V)$  curve along the voltage axis, because the properties of the voltage sensor, as evaluated by the  $Q(V)$ , are similar.

We, and others, have previously shown that different  $\beta$  subunits ( $\beta_{1a}$ ,  $\beta_{1b}$ ,  $\beta_{2a}$ ,  $\beta_{2b}$  and  $\beta_3$ ) and chimeric constructs among them when coexpressed with the  $\alpha_{1E}$  subunit or other  $Ca^{2+}$  channels share the common action of facilitating pore opening by shifting the activation curve to more negative potentials. On the other hand,  $\beta$  subunits can have an opposite effect on the voltage-dependent inactivation (Olcese *et al.* 1994). In this work, we have shown that the high coupling efficiency of the neuronal  $\alpha_{1E}$  is further improved by the  $\beta$  subunit. The tighter coupling caused by the  $\beta$  subunit results from a shift in the  $G(V)$  curve to more negative potentials, which reduces the gap between the  $Q(V)$  and the  $G(V)$  curves. However, this does not happen by heavily affecting the voltage sensitivity of the channel at negative potentials, since the feet of the  $G(V)$  curves for both  $\alpha_{1E}$  and  $\alpha_{1E} + \beta_{2a}$  are superimposed and the detection of the ionic current is close to  $-30$  mV for both types of channels. The tighter coupling correlates with the increase in the relative amplitude of the first, steeper component of the two components of the  $G(V)$  curve, from  $\sim 53$  to  $\sim 75\%$  of the total. Surprisingly we found that, in a range of potentials between 0 and 20 mV, the voltage dependence of the conductance of  $\alpha_{1E} + \beta_{2a}$  channels strictly follows the charge movement. In contrast, for the cardiac  $\alpha_{1C}$ , the voltage gap separating  $Q(V)$  and  $G(V)$  curves remains large even when coexpressed with the  $\beta$  subunit. The fact that  $Q(V)$  and  $G(V)$  curves are separated on the voltage axis can be explained by a sequential model with several closed states (C) and a final open state (O). Each transition between the conformational closed states along the activation pathway involves a discrete charge movement. Under these conditions, the  $Q(V)$  curve has to precede the  $G(V)$  curve, which represents the equilibrium between the open state and the closed states. The finding that in  $\alpha_{1E}$  the two curves,  $Q(V)$  and  $G(V)$ , lie so close on the voltage axis, suggests the presence of relatively few closed states or similarly that most of the charge is carried by transitions that are close to the last closed-to-open transition. The overlapping of the  $Q(V)$  and  $G(V)$  curves for potentials around 0 mV in  $\alpha_{1E} + \beta_{2a}$  channels, suggests that the channel at these potentials behaves like a

two-state channel (CO). In fact, a theoretical voltage-dependent ion channel able to swing between only two states (closed and open) would show superimposed  $Q(V)$  and  $G(V)$  curves. The physical counterpart of this result is a channel protein in which a small movement of the voltage sensor produces a large change in the open probability of the pore.

The coexpression of the  $\beta_{2a}$  subunit has a more remarkable effect on the  $\alpha_{1C}$  than on the  $\alpha_{1E}$  channel. The much smaller shift to the left of the  $G(V)$  curve of the  $\alpha_{1E}$  ( $-15$  mV) than of  $\alpha_{1C}$  (*ca*  $-50$  mV) channels, caused by  $\beta_{2a}$  coexpression, could be related to the intrinsic differences in voltage separation between the  $Q(V)$  and  $G(V)$  curves (20 mV for  $\alpha_{1E}$  and *ca* 100 mV for  $\alpha_{1C}$ ). We can speculate that the coupling efficiency between charge movement and channel opening in  $\alpha_{1E}$  is near maximal, making less evident the regulation by the  $\beta_{2a}$ , while the large voltage separation between  $G(V)$  and  $Q(V)$  of  $\alpha_{1C}$  leaves more room for regulation. We conclude that in the  $\alpha_{1C}$   $Ca^{2+}$  channel there are many closed states prior to channel opening and the charge movement is not tightly coupled to pore opening, while the opposite is true for  $\alpha_{1E}$ . Related to this result is the marked change in the time course that the  $\beta_{2a}$  causes in the installation of the  $\alpha_{1C}$  ionic current (Perez-Reyes *et al.* 1992), which it does not do when it is expressed with  $\alpha_{1E}$ .

The regulatory properties of  $\beta$  subunits have been studied in different expression systems and it is generally agreed that the expression of the  $\beta$  subunit either potentiates  $\alpha_1$  ionic current (Singer *et al.* 1991; Wei *et al.* 1991; Lacerda *et al.* 1991; Varadi *et al.* 1991; Neely *et al.* 1993) and/or increases the number of high-affinity dihydropyridine (DHP) binding sites (Lacerda *et al.* 1991; Varadi *et al.* 1991; Perez-García, Kamp & Marban, 1995). The mechanism by which these changes occur may vary in different clones and expression systems. Increased high-affinity binding and potentiation of ionic current could be due either to an increase of cell surface  $\alpha_1$  subunits or to stabilization of new conformations that show the potentiated ionic current and a shift in the equilibrium between low- (undetectable) and high-affinity DHP binding. Although the effect of the  $\beta$  subunit on the expression of  $\alpha_1$  was specifically addressed in two instances, the results reported were the opposite. Upon  $\beta$  subunit coexpression, Nishimura, Takeshima, Hofmann, Flockerzi & Imoto (1993) measured an increase in DHP binding to *Xenopus* membranes without changes in expression of  $\alpha_1$  assayed by Western blotting, while Josephson & Varadi (1996), studying the effect of the  $\beta$  subunit on  $\alpha_1$  function in HEK 293 cells reported an increase in both ionic current and amount of  $\alpha_1$ , assayed by measuring charge movement in  $\alpha_1 + \beta$ -expressing *vs.*  $\alpha_1$ -expressing cells. In other cases, it has been demonstrated that the enhancement of ionic current in *Xenopus* oocytes after coexpression of the accessory  $\beta$  subunit was not due to increased  $\alpha_1$  expression since the increase in the ionic current could be totally accounted for by an increase in the open probability of the

expressed channels (Neely *et al.* 1993; Shistik *et al.* 1995). In comparison, the  $\alpha_2\delta$  subunit alone has been shown to boost the expression of the  $\alpha_1$  subunit in *Xenopus* oocytes (Shistik *et al.* 1995).

In the present work, in batches of oocytes with very poor  $\alpha_{1E}$  expression,  $\beta_{2a}$  promoted an increase in the current level which can be accounted for by the increase in open probability (Noceti *et al.* 1996). On the other hand, in batches of oocytes with high  $\alpha_{1E}$  expression, the  $\beta_{2a}$  subunit induced a reduction of the total charge movement, suggesting a lower expression level. One possible explanation for this observation may be that in oocytes in which the  $\alpha_{1E}$  mRNA induces a saturating rate of protein synthesis, the coexpression of an additional protein, in this case  $\beta_{2a}$ , competes for the synthetic machinery and lowers the total number of  $\alpha_1$  subunits that are made.

- ALMERS, W. (1978). Gating currents and charge movements in excitatory membranes. *Reviews of Physiology, Biochemistry and Pharmacology* **82**, 96–190.
- ALMERS, W. & ARMSTRONG, C. M. (1980). Survival of K<sup>+</sup> permeability and gating currents in squid axons perfused with K<sup>+</sup>-free media. *Journal of General Physiology* **75**, 61–78.
- BARISH, M. E. (1983). A transient calcium-dependent chloride current in the immature *Xenopus* oocyte. *Journal of Physiology* **342**, 309–325.
- BEAN, B. P. & RIOS, E. (1994). Non linear charge movement in mammalian cardiac ventricular cell. Component from Na and Ca channels gating. *Journal of General Physiology* **94**, 65–93.
- CATTERALL, W. A. (1991). Functional subunit structure of voltage-gated calcium channels. *Science* **253**, 1499–1500.
- DELBONO, M., GOPALAKRISHNAN, A., NEELY, A., OLCESE, R., BIRNBAUMER, L. & STEFANI, E. (1994). Skeletal muscle calcium channel domain I slows down  $\alpha_1$  cardiac channel opening without changes in the voltage sensor. *Biophysical Journal* **66**, 88.
- DE WAARD, M. & CAMPBELL, K. P. (1995). Subunit regulation of the neuronal  $\alpha_{1A}$  Ca<sup>2+</sup> channel expressed in *Xenopus* oocytes. *Journal of Physiology* **485**, 619–634.
- HOFMANN, F., BIEL, M. & FLOCKERZI, V. (1994). Molecular basis for Ca<sup>2+</sup> channel diversity. *Annual Review of Neuroscience* **17**, 399–418.
- HULLIN, R., SINGER-LAHAT, D., FREICHEL, M., BIEL, M., DASCAL, N., HOFMANN, F. & FLOCKERZI, V. (1992). Calcium channel beta subunit heterogeneity: functional expression of cloned cDNA from heart, aorta and brain. *EMBO Journal* **11**, 885–890.
- JOSEPHSON, I. R. & VARADI, G. (1996). The  $\beta$  subunit increase Ca<sup>2+</sup> current and gating charge movement of human cardiac L-type Ca<sup>2+</sup> channels. *Biophysical Journal* **70**, 1285–1293.
- KAMP, T. J., PÉREZ-GARCÍA, M. T. & MARBAN, E. (1996). Enhancement of ionic current and charge movement by coexpression of calcium channel  $\beta_{1A}$  subunit with  $\alpha_{1C}$  subunit in a human embryonic kidney cell line. *Journal of Physiology* **492**, 89–96.
- LACERDA, A. E., KIM, H. S., RUTH, P., PEREZ-REYES, E., FLOCKERZI, V., HOFMANN, F., BIRNBAUMER, L. & BROWN, A. M. (1991). Normalization of current kinetics by interaction between the  $\alpha_1$  and  $\beta$  subunits of the skeletal muscle dihydropyridine-sensitive Ca<sup>2+</sup> channel. *Nature* **352**, 527–530.
- LEE, K. S. & TSIEN, R. W. (1982). Reversal of current through calcium channels in dialyzed single heart cells. *Nature* **297**, 498–501.
- LORY, P., VARADI, G., SLISH, D. F., VARADI, M. & SCHWARTZ, A. (1993). Characterization of beta subunit modulation of a rabbit cardiac L-type Ca<sup>2+</sup> channel alpha 1 subunit as expressed in mouse L cells. *FEBS Letters* **315**, 167–172.
- MANNUZZU, L. M., MORONNE, M. M. & ISACOFF, E. Y. (1996). Direct physical measure of conformational rearrangement underlying potassium channel gating. *Science* **271**, 213–216.
- NEELY, A., OLCESE, R., WEI, X., BIRNBAUMER, L. & STEFANI, E. (1994). Ca<sup>2+</sup>-dependent inactivation of a cloned cardiac Ca<sup>2+</sup> channel alpha 1 subunit ( $\alpha_{1C}$ ) expressed in *Xenopus* oocytes. *Biophysical Journal* **66**, 1895–1903.
- NEELY, A., WEI, X., OLCESE, R., BIRNBAUMER, L. & STEFANI, E. (1993). Potentiation by the  $\beta$  subunit of the ratio of the ionic current to the charge movement in the cardiac calcium channel. *Science* **262**, 575–578.
- NISHIMURA, S., TAKESHIMA, H., HOFMANN, F., FLOCKERZI, V. & IMOTO, K. (1993). Requirement of the calcium channel beta subunit for functional conformation. *FEBS Letters* **324**, 283–286.
- NOCETI, F., BALDELLI, P., WEI, X., QIN, N., TORO, L., BIRNBAUMER, L. & STEFANI, E. (1996). Effective gating charges per channel in voltage dependent K<sup>+</sup> and Ca<sup>2+</sup> channels. *Journal of General Physiology* **108**, 143–155.
- OLCESE, R., QIN, N., SCHNEIDER, T., NEELY, A., WEI, X., STEFANI, E. & BIRNBAUMER, L. (1994). The amino termini of calcium  $\beta$  subunits set rates of inactivation independently of their effect on activation. *Neuron* **13**, 1433–1438.
- PEREZ-GARCIA, M. T., KAMP, T. J. & MARBAN, E. (1995). Functional properties of cardiac L-type calcium channels transiently expressed in HEK293 cells. Roles of alpha 1 and beta subunits. *Journal of General Physiology* **105**, 289–305.
- PEREZ-REYES, E., CASTELLANO, A., KIM, H. S., BERTRAND, P., BAGGSTROM, E., LACERDA, A. E., WEI, X. & BIRNBAUMER, L. (1992). Cloning and expression of cardiac/brain  $\beta$  subunit of the L-type calcium channel. *Journal of Biological Chemistry* **267**, 1792–1797.
- PEREZ-REYES, E., KIM, H. S., LACERDA, A. E., HORNE, W., WEI, X., RAMPE, D., CAMPBELL, K. P., BROWN, A. M. & BIRNBAUMER, L. (1989). Induction of calcium current by the expression of the  $\alpha_1$ -subunit of the dihydropyridine receptor from skeletal muscle. *Nature* **340**, 233–236.
- RAKOWSKI, R. F. (1993). Charge movement by the Na/K pump in *Xenopus* oocytes. *Journal of General Physiology* **101**, 117–144.
- SANFORD, J., CODINA, J. & BIRNBAUMER, L. (1991). Gamma-subunits of G proteins, but not their alpha- or beta-subunits, are polyisoprenylated. Studies on post-translational modifications using *in vitro* translation with rabbit reticulocyte lysates. *Journal of Biological Chemistry* **266**, 9570–9579.
- SCHNEIDER, T., WEI, X., OLCESE, R., COSTANTIN, J. L., NEELY, A., PALADE, P., PEREZ-REYES, E., QIN, N., ZHOU, J., CRAWFORD, G. D., SMITH, R. G., APPEL, S. H., STEFANI, E. & BIRNBAUMER, L. (1994). Molecular analysis and functional expression of the human type E neuronal Ca<sup>2+</sup> channel  $\alpha_1$ -subunit. *Receptors and Channels* **2**, 255–270.
- SCHOPPA, N. E., MCCORMACK, K., TANOUYE, M. A. & SIGWORTH, F. J. (1992). The size of gating charge in wild-type and mutant *Shaker* potassium channels. *Science* **255**, 1712–1715.
- SHISTIK, E., IVANINA, T., PURI, T., HOSEY, M., & DASCAL, N. (1995). Ca<sup>2+</sup> channel enhancement by  $\alpha_2/\delta$  and  $\beta$  subunits in *Xenopus* oocytes: contribution of changes in channel gating and  $\alpha_1$  protein level. *Journal of Physiology* **489**, 55–62.

- SINGER, D., BIEL, M., LOTAN, I., FLOCKERZI, V., HOFMANN, F. & DASCAL, N. (1991). The roles of the subunits in the function of the calcium channel. *Science* **253**, 1553–1557.
- STEA, A., DUBEL, S. J., PRAGNELL, M., LEONARD, J. P., CAMPELL, K. P. & SNUTCH, T. P. (1993). A beta-subunit normalizes the electrophysiological properties of a cloned N-type  $\text{Ca}^{2+}$  channel alpha 1-subunit. *Neuropharmacology* **32**, 1103–1116.
- STEFANI, E., TORO, L., PEROZO, E. & BEZANILLA, F. (1994). Gating of *Shaker*  $\text{K}^+$  channels: I. Ionic and gating currents. *Biophysical Journal* **66**, 996–1010.
- VARADI, G., LORY, P., SCHULTZ, D., VARADI, M. & SCHWARTZ, A. (1991). Acceleration of activation and inactivation by the beta subunit of the skeletal muscle calcium channel. *Nature* **352**, 159–162.
- WEI, X. Y., NEELY, A., OLCESE, R., STEFANI, E. & BIRNBAUMER, L. (1996). Increase in  $\text{Ca}^{2+}$  channel expression and modification of activation kinetics by deletions at the amino terminus of the cardiac  $\alpha_{1C}$  subunit. *Receptors and Channels* (in the Press).
- WEI, X. Y., PEREZ-REYES, E., LACERDA, A. E., SCHUSTER, G., BROWN, A. M. & BIRNBAUMER, L. (1991). Heterologous regulation of the cardiac  $\text{Ca}^{2+}$  channel  $\alpha_1$  subunit by skeletal muscle  $\beta$  and  $\gamma$  subunits. Implication for the structure of cardiac L-type  $\text{Ca}^{2+}$  channels. *Journal of Biological Chemistry* **266**, 21943–21947.
- WILLIAMS, M. E., FELDMAN, D. H., McCUE, A. F., BRENNER, R., VELICELEBI, G., ELLIS, S. B. & HARPOLD, M. M. (1992). Structure and functional expression of alpha 1, alpha 2, and beta subunits of a novel human neuronal calcium channel subtype. *Neuron* **8**, 71–84.

#### Acknowledgements

This work was supported by NIH grants AR38970 to E.S. and AR43411 to L.B. and it was done during the tenure of a Grant-in-Aid 1113-GI1 award to R.O. from the American Heart Association, Greater Los Angeles Affiliate.

#### Author's email address

E. Stefani: estefani@anes.ucla.edu

Received 29 May 1996; accepted 9 September 1996.